

Humming Trains in Seismology: An Opportune Source for Probing the Shallow Crust

Laura Pinzon-Rincon^{*1}, François Lavoué¹, Aurélien Mordret¹, Pierre Boué¹, Florent Brenguier¹, Philippe Dales^{1,2}, Yehuda Ben-Zion³, Frank Vernon⁴, Christopher J. Bean⁵, and Daniel Hollis⁶

Abstract

Seismologists are eagerly seeking new and preferably low-cost ways to map and track changes in the complex structure of the top few kilometers of the crust. By understanding it better, they can build on what is known regarding important, practical issues. These include telling us whether imminent earthquakes and volcanic eruptions are generating telltale underground signs of hazard, about mitigation of induced seismicity such as from deep injection of wastewater, how the Earth and its atmosphere couple, and where accessible natural resources are. Passive seismic imaging usually relies on blind correlations within extended recordings of Earth's ceaseless "hum" or coda of well-mixed, small vibrations. In this article, we propose a complementary approach. It is seismic interferometry using opportune sources—specifically ones not stationary in time and moving in a well-understood configuration. Its interpretation relies on an accurate understanding of how these sources radiate seismic waves, precise timing, careful placement of pairs of listening stations, and seismic phase differentiation (surface and body waves). Massive freight trains were only recently recognized as such a persistent, powerful cultural (human activity-caused) seismic source. One train passage may generate a tremor with an energy output of a magnitude 1 earthquake and be detectable for up to 100 km from the track. We discuss the source mechanisms of train tremors and review the basic theory on sources. Finally, we present case studies of body- and surface-wave retrieval as an aid to mineral exploration in Canada and to monitoring of a southern California fault zone. We believe noise recovery from this new signal source, together with dense data acquisition technologies such as nodes or distributed acoustic sensing, will deeply transform our ability to monitor activity in the shallow crust at sharpened resolution in time and space.

Cite this article as Pinzon-Rincon, L., F. Lavoué, A. Mordret, P. Boué, F. Brenguier, P. Dales, Y. Ben-Zion, F. Vernon, C. J. Bean, and D. Hollis (2021). Humming Trains in Seismology: An Opportune Source for Probing the Shallow Crust, *Seismol. Res. Lett.* **92**, 623–635, doi: [10.1785/0220200248](https://doi.org/10.1785/0220200248).

Introduction

Vehicle traffic was long seen mainly as a pervasive source of nuisance noise that degrades seismic records (Douze and Laster, 1979). However, the recent and intriguing discovery of tremors from trains startled seismologists. Studies soon followed on detection and characterization of these signals (Riahi and Gerstoft, 2015; Green *et al.*, 2017; Fuchs *et al.*, 2018; Inbal *et al.*, 2018; Li *et al.*, 2018) as well as source modeling (Lavoué *et al.*, 2020). Earlier studies of Nakata *et al.* (2011), Chang *et al.* (2016), and Quiros *et al.* (2016) proposed using traffic noise and seismic interferometry for both body- and surface-wave imaging. These studies were, however, limited to highly local sources of background cultural noise and near-surface applications.

In a fortuitous attempt to gather nonvolcanic tremors (NVTs) along the San Andreas fault zone in southern California, Inbal *et al.* (2018) discovered extended tremor sequences that shared puzzling similarities with NVTs. However, they traced the new discovery to massive freight

1. Univ. Grenoble Alpes, Univ. Savoie Mont Blanc, CNRS, IRD, UGE, ISTerre, Grenoble, France; 2. Institute of Mine Seismology, Greater Sudbury, Ontario, Canada;

3. Department of Earth Sciences and Southern California Earthquake Center, University of Southern California, Los Angeles, California, U.S.A.; 4. IGPP, University of California, San Diego, La Jolla, California, U.S.A.; 5. Geophysics Section, Dublin Institute for Advanced Studies, Dublin, Ireland; 6. Sisprobe, Grenoble, France

*Corresponding author: laura-alejandra.pinzon-rincon@univ-grenoble-alpes.fr

© Seismological Society of America

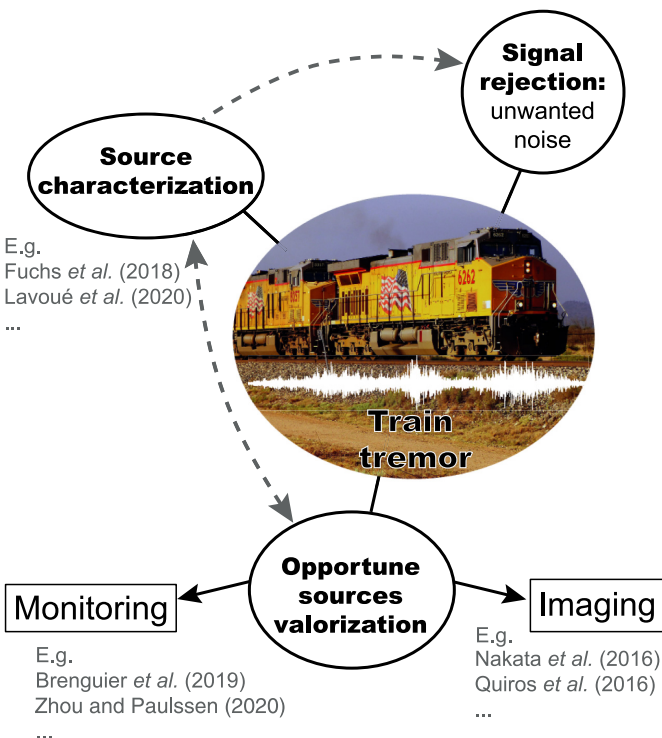


Figure 1. Example representation of studies related to train seismic tremors. The color version of this figure is available only in the electronic edition.

trains running along the nearby Coachella Valley. They could detect them as much as 100 km from the rails. [Brenguier et al. \(2019\)](#) calculated that a single 1 km long freight train rolling through a 10 km long railway section radiates energy equivalent to a magnitude 1 earthquake. Further using seismic interferometry for correlation of this underfoot train noise, [Brenguier et al. \(2019\)](#) and [Dales et al. \(2020\)](#) showed that it was possible to extract useful information on the Earth's crustal structure and temporal changes down several kilometers, which provides a potential alternative to costly monitoring of active sources such as hydraulic thumping or explosives ([Tsuji et al., 2018](#)).

This article reviews basic concepts and examples of the application of seismic interferometry to train tremors. Its special focus is on long-range body-wave retrieval for crustal exploration and monitoring (Fig. 1). The Green's function is the elastic impulse response of the ground between a seismic source and a seismic receiver, that is, the signature of the ground structure encapsulated by its effects on the velocity and other behaviors of a signal as it travels. Seismic interferometry is often able, by correlating diffuse coda or seismic noise, to retrieve the Green's function between two seismic sensors by turning one sensor into a virtual source. The impact of the Green's function retrieval in recent decades has been revolutionary (e.g., [Campillo and Paul, 2003](#); [Snieder, 2004](#);

[Wapenaar, 2004](#); [Shapiro et al., 2005](#)). It spurred publication of at least 2000 seismology articles in the last 15 yr. One payoff from seismic interferometry and Green's function retrieval is improved crustal imaging through correlation of pervasive surface-wave noise generated in the oceans in the period range from 1 to 20 s. Recent studies have also unveiled the possibility of reconstructing body waves at global (e.g., [Poli et al., 2012](#); [Boué et al., 2013](#)) and local scales ([Draganov et al., 2009](#); [Nakata et al., 2015, 2016](#); [Olivier et al., 2015](#)).

A perfect application of Green's function retrieval and seismic interferometry requires correlation of either a fully diffused seismic wavefield or noise signals generated from all around the studied region, including at depth ([Wapenaar, 2004](#)). In practice, these demands are never met. Seismologists must live with or find workarounds for partial reconstructions and potentially biased wave travel times ([Snieder et al., 2006](#); [King and Curtis, 2012](#)). Moving trains are welcome, opportune sources of noise on well-mapped railways. It is essential that they be rigorously assessed for seismic interferometry. Train traffic noise cannot be blindly correlated without considering the effects of irregular source distribution on body-wave retrieval.

In this article, we first describe typical train noise signals, discuss recent models of mechanisms that create train seismic radiations, and provide a map of the predicted extent of useful train noise in the contiguous United States. Second, we propose a methodological framework focusing our approach on the stationary zones (geographical area where we observe constructive interferences when cross-correlating signals between two stations, [Snieder, 2004](#)) and propose a signal processing strategy for applying seismic interferometry to train noise with a focus on long-range body-wave retrieval. We finally review two recent case studies regarding mineral exploration in Canada and tectonic fault monitoring in Southern California.

The Sound of Trains in the Earth

As noted, massive freight trains generate seismic waveforms with striking similarity to episodic tectonic tremors. These may be from such events as slow-slip fault motion (Fig. 2a). As [Inbal et al. \(2018\)](#) report, the identity of the sources as man-made was not obvious because freight train traffic often lacks cultural diurnal or weekly modulation and typical train speed (25 m/s or 90km/h) is in the range of reported tectonic tremor migration velocity at depth. However, train hum has a distinct signature with clear spectral lines above 1 Hz ([Fuchs et al., 2018](#)), as illustrated in Figure 2 for a train signal recorded in Canada about 3 km from the railway (first case study, see the [Body- and Surface-Wave Retrieval from Correlations of Train Tremors Applied to Mineral Exploration](#) section).

The engineering community has studied train-induced ground vibrations thoroughly to damp them and mitigate potential hazards. Several source mechanisms are under study (e.g., [Connolly et al., 2015](#)) including quasistatic excitation due

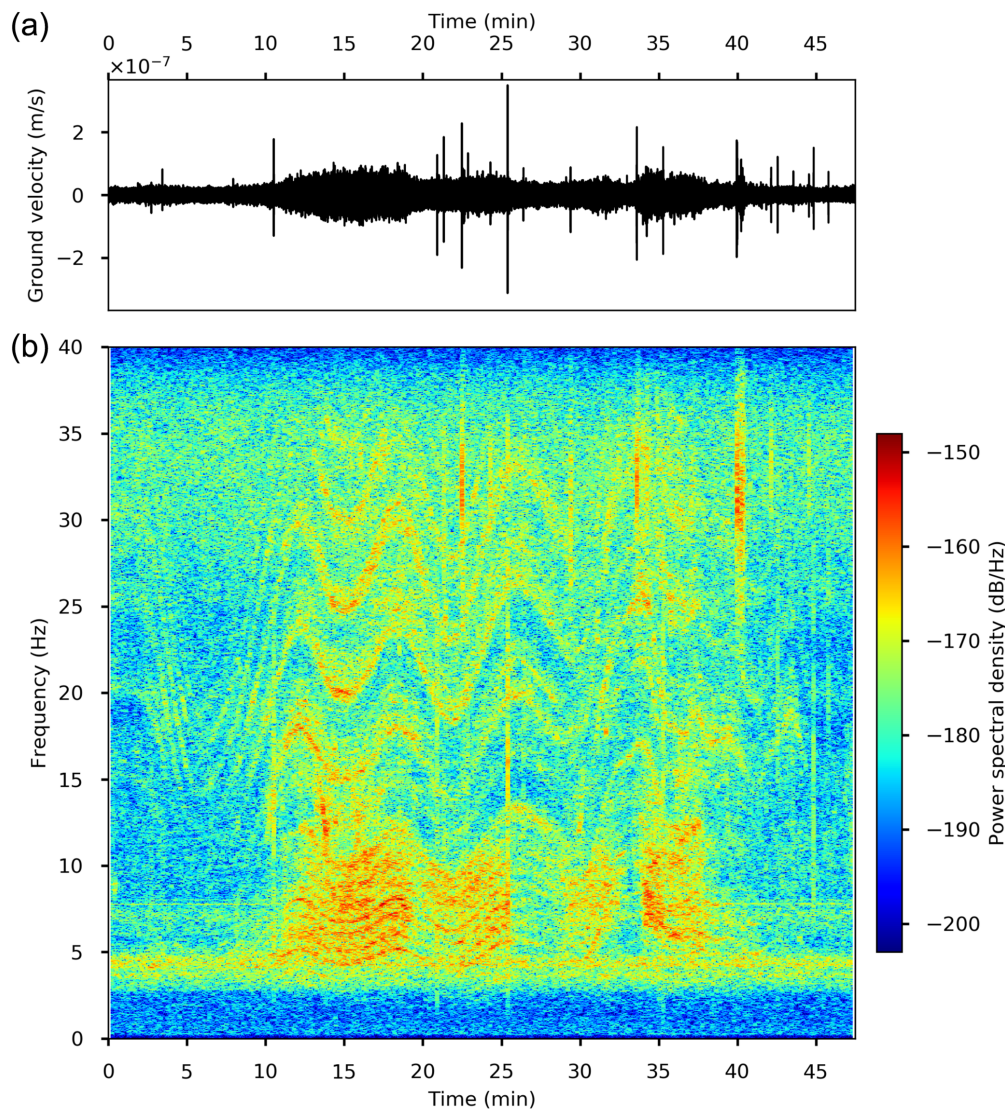


Figure 2. (a) A train tremor recorded 3 km away from a seismic station in Marathon, Canada. (b) Spectrogram showing clear spectral lines oscillating as train speed varies. The color version of this figure is available only in the electronic edition.

to axle loads and dynamic interactions among trains, tracks, and ground. In a recent study, Lavoué *et al.* (2020) showed that excitation due to axle loads is the main mechanism producing the spectral characteristics of seismic signals at intermediate to long distances from the railway (from hundreds of meters to tens of kilometers, Fuchs *et al.*, 2018; Inbal *et al.*, 2018; Li *et al.*, 2018; Brenguier *et al.*, 2019). One may then model train-generated seismic signals by considering only the vertical forces due to loading applied by axles on the railroad ties (commonly called sleepers) along the railway (Krylov and Ferguson, 1994; Lavoué *et al.*, 2020).

Lavoué *et al.* (2020) conclude that the spectral lines arise from complex interactions of periodic loads through the regularly spaced wheels on the more evenly separated sleepers. The frequencies of these spectral lines depend on train geometry

(trains traveling across rock or stiff soil generate higher-frequency and higher-amplitude signals). This ground stiffness parameter may also reflect a coupling between the rail track and the ground. Although maximum detection distance may be limited (a few kilometers) in sedimentary basins due to attenuation and weak excitation, again, it can reach almost 100 km on a hard-rock substratum. In southern California, for instance, Inbal *et al.* (2018) observed a freight train-tremor signal from as far as 90 km from the railway. At 45 km from the railway, they estimated a PGV of about 6×10^{-8} m/s. By applying a simple correction for intrinsic attenuation and geometrical spreading for body (*P*) waves, we now estimate that the level of PGV for a specific Coachella Valley train would be on the order of 5×10^{-7} m/s at 10 km and 5×10^{-6} m/s at 1 km. These values are quite low. Even high-sensitivity

(i.e., train car length and wheel spacing within each car), spacing between sleepers, and train velocity. We provide an open-source code to assess the frequency response of a specific train (see [Data and Resources](#)). With most trains, the dominant spectral lines are expected in the 1–20 Hz range, which is ideal for both high-frequency surface-wave tomography of the near subsurface and crustal body-wave imaging and monitoring (wavelengths not too large and scattering not too strong, Brenguier *et al.*, 2019).

Our ability to predict the long-range, body-wave peak ground velocity (PGV) of a moving train tremor—the physical motion in the medium as signals go through it—is crucial to image formation and monitoring any changes with seismic interferometry. Lavoué *et al.* (2020) proposed that train tremor PGV is directly proportional to the wagon weight for a given train length and is a square-root function of train length for constant wagon weight. Faster trains also generate higher PGVs. Moreover, the ground stiffness beneath railways controls high-frequency content and amplitude of excitation

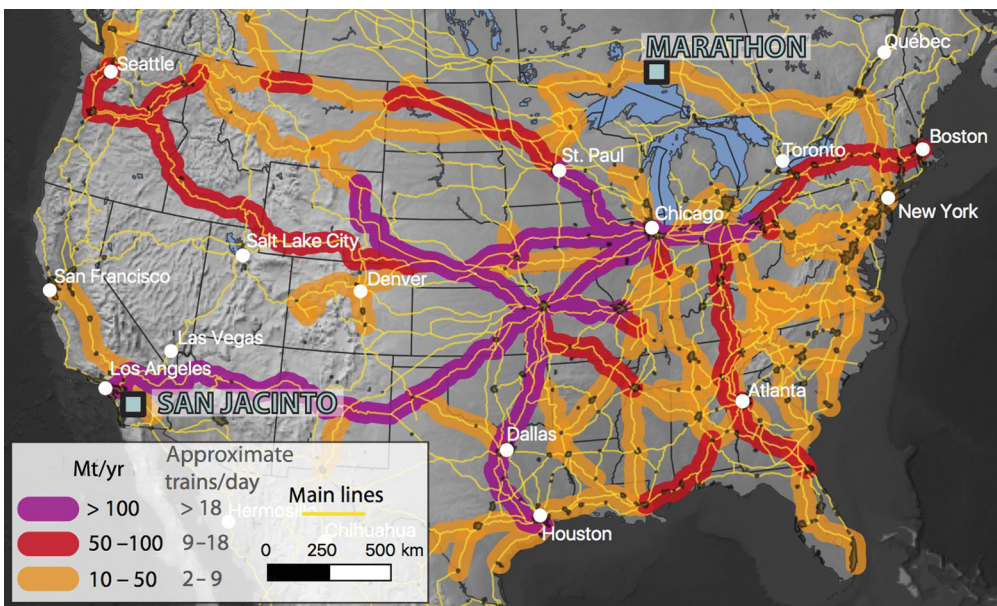


Figure 3. Regions of potential long-range train-tremor detection from the main railway route and annual tonnage information in North America. Colors represent annual freight tonnage, which is an indication of the number of trains traveling on the rail sections (sections with annual tonnage < 10 Mt/yr are ignored). Colored lines are 100 km thick, which is an indication for the distance from which we may detect individual train tremors (50 km from the railway, see details in [The Sound of Trains in the Earth](#) section).

seismometers may record such train signals at long distances only in quiet environments. Nevertheless, Brenguier *et al.* (2019) demonstrated that Coachella Valley train noise supported seismic body-wave interferometry—with data recorded by an array of geophones (nodes)—as much as 60 km from the railway (see the [Retrieving Long-Range Body Waves from Train-Tremor Correlations to Monitor the San Jacinto Fault Zone \(SJFZ\)](#) section).

At shorter distances, small-amplitude body waves might be barely visible in the raw data, either because surface waves hide them or because they are below the ambient noise level. However, it should be possible to extract body waves from the correlations of train tremors by stacking data from several passages (see the [Body- and Surface-Wave Retrieval from Correlations of Train Tremors Applied to Mineral Exploration](#) section). Using train tremors for seismic interferometry thus depends both on detection limits (instrument sensitivity and local noise level) and on reliably recognizable features in train signals.

Observation from previous studies (Inbal *et al.*, 2018; Brenguier *et al.*, 2019) persuades us that 50 km is a typical maximum distance range for detecting tremors generated from large North American freight trains. This led us to look into the spatial extent of detectable train tremor in the entire contiguous United States plus southern Canada (Fig. 3). The map displays the main freight railway routes. The swatches in colors

represent high tonnage routes. Their width (100 km) is a rough guide to potential long-range train-tremor detection scope. This map does not take into account the reduced detectability of signals in urban areas due to intense local noise or in sedimentary basins with strong attenuation compared with the southern California–Coachella Valley reference.

It is noteworthy that the Coachella Valley, a stretch of Sonoran Desert northwest of the Salton Sea, is a singularly apt place to find practical uses for ground vibrations of massive trains. Its Union Pacific railroad tracks are a prime corridor to and from the ports of Los Angeles and Long Beach, the western Hemisphere's busiest seaport complex. Dozens of trains go through daily. The average length is more than 2.5 km with more than

cars, often including multiple engines in front and back. Rail enthusiasts visit to make, and often to post on YouTube, mesmerizing videos of the immense steel caravans rumbling by (see [Data and Resources](#)).

Annual freight tonnage (Fig. 3) is a proxy for the number of trains traveling on rail sections. Assuming an average train length of 2 km and a weight of 15 kt (according to statistics derived from the public waybill samples, 2018, see [Data and Resources](#)), a tonnage of 100 Mt/yr corresponds to about 18 trains per day. The number of trains per day will affect the ability to stack the reconstructed body waves from seismic interferometry. It also affects the temporal resolution needed in monitoring applications (see the [Retrieving Long-Range Body Waves from Train-Tremor Correlations to Monitor the San Jacinto Fault Zone \(SJFZ\)](#) section). This map highlights the potential of using trains as sources of opportunity. Potential application may be in Cascade volcanoes, southern California's San Andreas fault system, induced seismicity (e.g., Oklahoma), and resource exploration and monitoring (minerals and water).

Seismic Interferometry with Opportune Sources

Seismic interferometry is a general term embracing all methodologies aiming to infer seismic responses from the correlation of seismic signals observed at multiple receiver locations (e.g., Wapenaar, Draganov, *et al.*, 2010; Wapenaar, Slob, *et al.*, 2010).

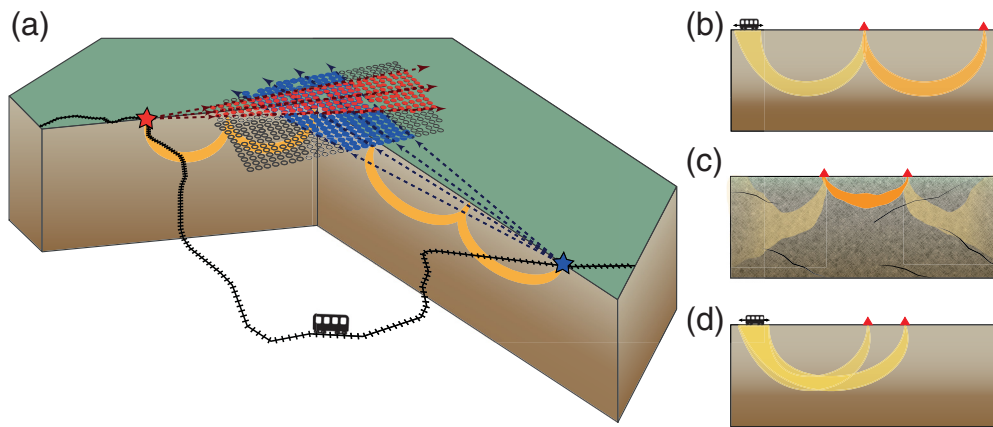


Figure 4. Schematic representation of seismic interferometry for opportune sources. (a) A railway surrounding a dense geophone array; an example from the Marathon (Canada) deployment. Different train locations (stars) allow for the illumination of the array with different azimuths. Yellow kernels are schematic views of the propagation of diving P waves. (b–d) Three different scenarios of wave interference: (b,c) leading to a proper measurement of a diving P wave and (d) leading to a spurious or virtual refraction measurement.

To turn sensors into virtual sources, this concept has been refined in seismology and seismic exploration, mostly in the past 20 yr, based on the pioneering studies of random fields or vertical planar-wave autocorrelation (Aki, 1957; Claerbout, 1968) and the time-reversal principle in acoustics (Fink, 1997).

To retrieve a Green's function using the correlation or an equivalent operator, the theory heavily relies on either a stationary phase condition (e.g., Snieder, 2004; Roux *et al.*, 2005) and/or an equipartition of modes defining a diffuse field (e.g., Sánchez-Sesma and Campillo, 2006). The stationary phase condition implies that the correlation function's convergence toward the Green function requires the presence of sources (or scatterers) in line with two carefully placed receivers. In a 2D homogeneous medium, these stationary points define a hyperbolic area, outward from the receiver pair, with an aperture that is frequency dependent (the lower the frequency is, the broader the calculated source region is). Also known as Fresnel zones, these “kernels” are clues to the reliability of the correlation's implied source locations. In 3D and for both surface- and body-wave retrieval, the requirement of equipartition remains. Full Green's function retrieval demands sources that are evenly distributed along an arbitrarily shaped surface enclosing the two sensors (e.g., Wapenaar, 2004; Wapenaar and Fokkema, 2006). However, even with a clearly dominant distribution of sources at the free surface, several studies confirmed the feasibility of retrieving body waves (e.g., Draganov *et al.*, 2009, 2013) and even explicitly using traffic noise (Nakata *et al.*, 2011).

Each of the possible phases (or wave types) included in the Green's function has its own source sensitivity. The main contributors to a particular phase are sources within its stationary

phase area. We can therefore measure a specific phase between two receivers by correlation of a source within its stationary phase zone including the surface. The following case studies investigated P waves from moving trains and emerging from the interference between a direct P recorded at the first station and a PP (redirected once by a buried layer or formation edge) recorded by a second station after a rebound below the first one. One can do the same with S waves (see Fig. 4b).

Useful interference occurs if the seismic sources (trains) satisfy the stationary phase criterion:

$$\Delta t = t_{pp} - t_p \leq t_{\text{Green}} \pm \frac{T}{4}, \quad (1)$$

in which t_{pp} is the arrival time of the PP wave at the second receiver, t_p is the arrival time of the P wave at the first station, t_{Green} is the arrival time of the P wave between the two receivers, and T is the dominant period. Using sources controlled by some means to retrieve the body-wave response through interferometry is similar to daylight imaging developed by (Schuster *et al.*, 2004) or to the virtual source approach discussed by (Bakulin and Calvert, 2006) for borehole imaging. For train signals, we need to characterize the source and of course take into account that the sources are moving.

One reason that train signals are practical for interferometric studies is that we can easily detect, or learn in advance, that a train is coming. If a railway is sufficiently close to a targeted area, a single train's motion could illuminate many azimuths and potentially different depths. Figure 4a shows an example of geometry in Marathon, Ontario, Canada. At this site, a railway essentially surrounds a temporary array put in to image an ore deposit (detailed in the following section). By selecting station pairs aligned with train locations (illustrated for two positions by red and blue stars), one can potentially illuminate the ore body from a broad azimuth range. Figure 4b–d is a schematic of several P -wave interference scenarios, each with a pair of stations. They offer a perfect ballistic interference between a diving P and PP wave (Fig. 4b) leading to a directly measurable diving P wave between the two receivers and a classical scenario of a scattered wavefield from which we expect some random source energy to transit between the two receivers (Fig. 4c); see also a more problematic interference between

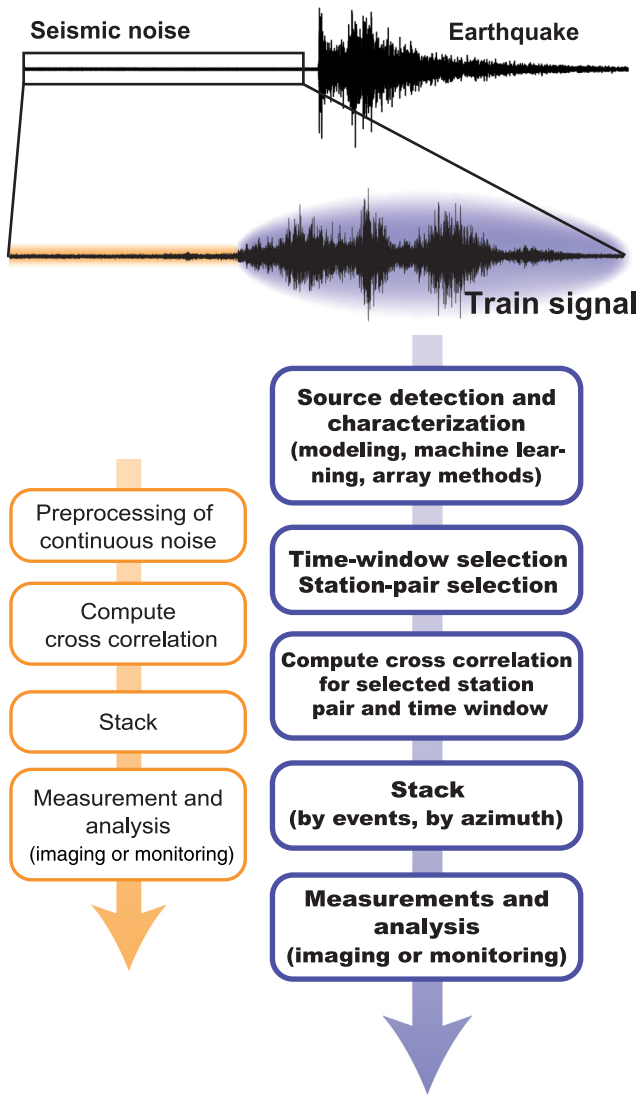


Figure 5. Chart illustrating the processing steps for opportune sources (in blue) compared with the standard ambient noise correlation workflow (in orange). The color version of this figure is available only in the electronic edition.

two diving waves or a head wave recorded at the two stations (Fig. 4d). Instances of this last scenario are sometimes regarded as spurious correlations or virtual refractions (Dong *et al.*, 2006; Snieder *et al.*, 2006; Mikesell *et al.*, 2009). Although not included within the impulse response between the two stations, this last correlation feature might be useful for imaging if it is well distinguished from expected diving waves (Dong *et al.*, 2006).

We decided to try to illuminate specific ray paths using a data-processing workflow, starting with the selection of short time windows including specific train passages. This presumably could be extended to any kind of seismic tremor and should help extract body waves between well-selected pairs of stations useful for imaging and monitoring studies.

Strategy for Data Processing

Standard noise-correlation workflow typically removes strong transient events such as earthquakes and then correlates the entire remaining time series recorded at different sensors (Bensen *et al.*, 2007). With opportune sources including train traffic, we propose a novel workflow. It includes source characterization with signal and station pair selections as alternatives to blind correlation. We thus aim to improve the signal-to-noise ratio (SNR) of the reconstructed correlation functions and the temporal resolution of monitoring studies. This approach is illustrated in the [Body- and Surface-Wave Retrieval from Correlations of Train Tremors Applied to Mineral and Retrieving Long-Range Body Waves from Train-Tremor Correlations to Monitor the San Jacinto Fault Zone \(SJFZ\)](#) sections for imaging and monitoring applications, respectively. Figure 5 summarizes the five main stages of our data processing in comparison with the classical method of continuous blind data correlation.

The workflow's steps are as follows:

1. Identification: identify opportune source signatures in the continuous data and, if possible, locate these sources perhaps by distance but at least in azimuth. As shown in [The Sound of Trains in the Earth](#) section, the modeling of opportune sources helps reveal the temporal and spectral content of the generated wavefield. Standard (short-time average window/long-time average window) and more advanced techniques (e.g., Kong *et al.*, 2019; Meng *et al.*, 2019) detect these transient events. Array processing techniques (e.g., Cheng *et al.*, 2020) can be used to locate their sources.
2. Station-pair selection: with source location estimates in mind, narrow down the options for station pairs. For a given signal time window, only station pairs for which the train source is in a stationary phase zone are used. During a train passage, the energy carried by its seismic signal reaches an array of sensors from a range of directions. Figure 4a illustrates two train positions at different times (red and blue stars) and the associated selected stations for pair-wise correlations (red and blue dots).
3. Computation: compute cross correlations after proper time windowing and station pairs selection.
4. Stacking (by events and by azimuth): to improve SNR, stack the cross correlations over different events. Cultural sources such as train traffic have the advantages of reliability and frequent repetition.
5. Measurement and analysis: depending on the type of studies, various approaches such as travel-time measurements can enhance imaging and monitoring applications.

Body- and Surface-Wave Retrieval from Correlations of Train Tremors Applied to Mineral Exploration

We investigated a region near Marathon (see Fig. 6b) where potential targets include a high concentration of platinum

group metals and minor Cu in a gabbro intrusion. Reconstruction of high-frequency body waves from train noise correlations was of significant interest. This is because such signals' sharp sensitivity to seismic velocity contrasts at depth, offering a clear path to imaging geological boundaries. In the fall of 2018, we deployed 1010 seismic station in a backbone array and a dese staion line (see Fig. 6b). We recorded 30 straight days of seismic signals.

Dales *et al.* (2020) showed that the main generators of high-frequency seismic noise in Marathon are freight trains to the southwest. They reinforced earlier evidence that, by selectively using train traffic noise, one retrieves body waves better than by correlating a more extended or full noise record. Dales *et al.* (2020) stacked correlations over one month, selecting all periods during which the ambient noise came from the direction aligned with a dense west–east line of sensors. Their study is illustrative but the results did not allow them to perform 3D imaging. We moved a step further by separating and binning noise azimuths for virtual source retrieval in different directions. Following the workflow proposed in the [Strategy for Data Processing](#) section, we detected train passages, inferred the positions and azimuths of the trains relative to the array, carefully selected station pairs and time windows for correlations, and finally stacked by train passage and azimuth.

A more detailed workflow follows:

1. We first generated a catalog of train passages with the covariance matrix method proposed by Seydoux *et al.* (2016). This method uses the spatial coherence of the signals to detect emergent signals in the noise. We applied the procedure to the entire dataset day by day and detected 207 train passages in 30 days. We retained for studying ~180 events after skipping overlapping trains. Beamforming concluded that the array receives energy from each train for an ~80 min.
2. Second, we extracted train signals from the rest of the recording and selected station pairs in line with train positions. To determine position, we did beamforming in 1 min long windows using data filtered between 8 and 17 Hz (Fig. 6d,e, right, shows six beamforming panels for six different events at two different times). Each panel corresponds to a 1 min beamforming time window and one single train passage. We saw that, with properly selected time windows for each event, we got tight and usable ranges of azimuth. We assumed that the main source of energy was the train and noted the maximum beam power. We back-projected this signal onto the railway to locate each train minute by minute. Figure 6b (red and blue crosses) shows the train position from the first beamforming panel (i.e., one single train). We then selected station pairs that are in line with the train position for each minute, always taking the station closest to the railway as a virtual source (red and blue arrows in Fig. 6b). We applied an azimuthal filter of ±5° for each station pair with respect to the train position.

3. Third, we cross correlated the selected station pairs minute by minute without overlap and for each event (i.e., train passage). Filters excluded signals outside 15–40 Hz to avoid surface waves. We stacked cross correlations according to their interstation distances and collected them in distance-binned correlation gathers for the selected station pairs (step 2). In contrast, Figure 6a shows the stack of 1 min cross correlation for a quiet period (i.e., nontrain passage), highlighting the absence of coherent wave propagation in this rather high-frequency window.
4. In the fourth and last step, we stacked events sharing the same train azimuth. We stacked these correlation gathers into a reference azimuthal gather. We converged on a stable reference stack from six train passages. We showed that by applying the workflow explained in the [Strategy for Data Processing](#) section, we only needed 1 min of data and stacking over the six events to retrieve body waves. Figure 6d,e, left, shows the stacked section over six train passages with 1 min data segments.

We retrieved two dominant arrivals with an apparent velocity of 3.8 and 7 km/s. There are uncertainties, but we suggest that the first arrival is a *P* wave, and the second one is probably a mix of *S* and surface waves. One can use both *P*- and *S* waves plus high-frequency surface waves jointly for imaging the subsurface. We need further analysis to assess the types of body waves (direct and refracted) and how one can use velocity variations in the azimuth's function for 3D imaging.

Retrieving Long-Range Body Waves from Train-Tremor Correlations to Monitor the San Jacinto Fault Zone (SJFZ)

Following studies by Nakata *et al.* (2015, 2016) of high-frequency body-wave retrieval using dense seismic receiver arrays, Brenguier *et al.* (2020), Takano *et al.* (2020), and Zhou and Paulsen (2020) explored ways to monitor temporal changes of ballistic wave velocities. In this section, we employ opportune seismic sources to passively monitor temporal changes and revisit the experiment of Brenguier *et al.* (2019). Here, the goal was to use ballistic *P* waves, reconstructed from ambient vibrations between two dense arrays, to monitor subtle velocity changes at depth within the SJFZ (parallel to the San Andreas and part of the same fault complex).

Brenguier *et al.* (2019) showed that standard ambient-noise-correlation processing can retrieve high-frequency direct *P* waves that traveled between two arrays, one at Piñon Flat Observatory (PFO) and the other on the Cahuilla Reservation (CIR, Fig. 7). The main sources of these *P* waves were Coachella Valley freight trains traversing the Coachella Valley about 30 km to the east–northeast of PFO. Brenguier *et al.* (2019) used full records of ambient noise to obtain stable direct *P*-wave seismograms. We showed that, by carefully selecting time windows in which most

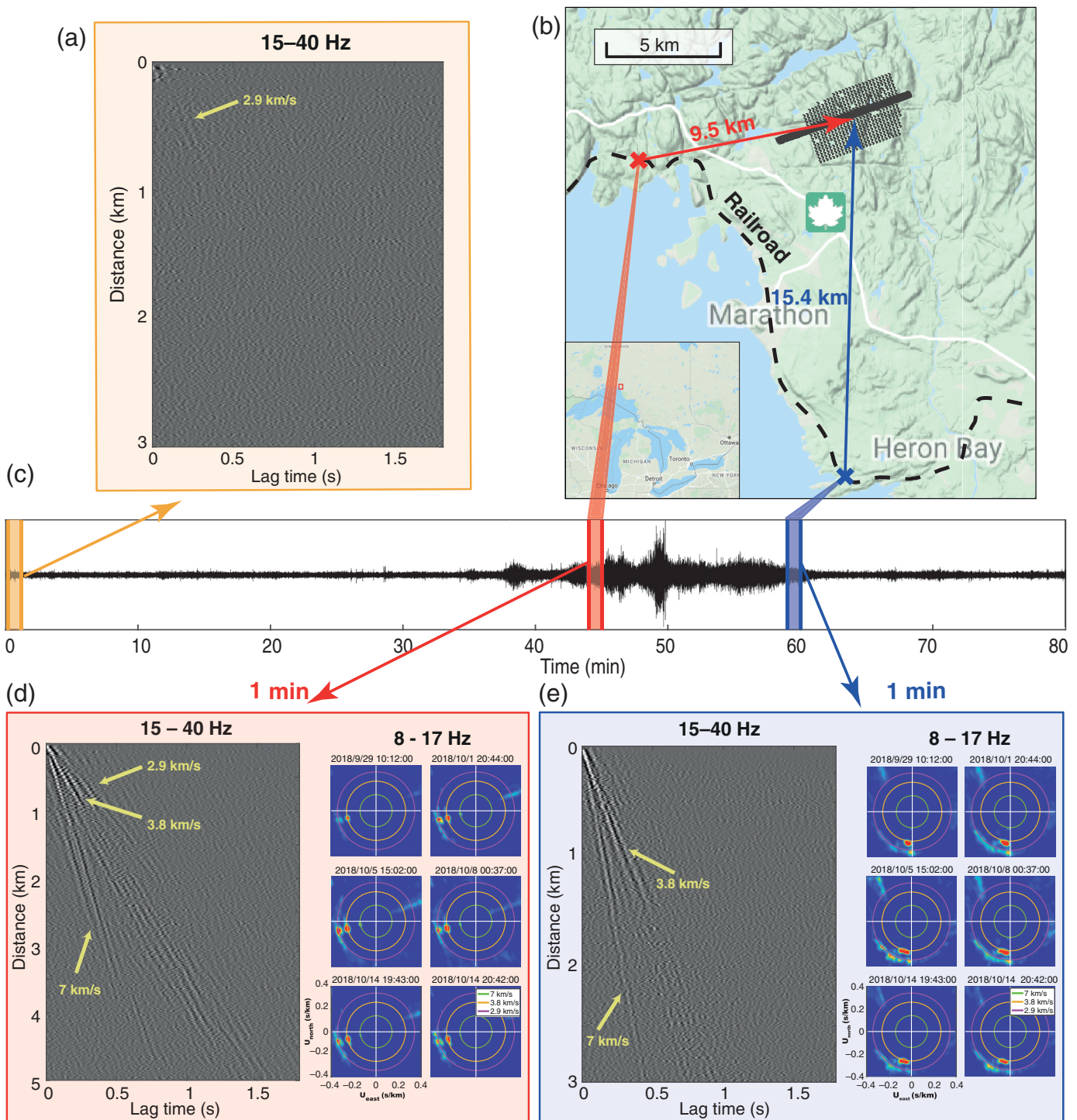


Figure 6. Case studies of train-tremor correlations over a dense array at Marathon, Canada. (a) 1 min cross correlation for a quiet time period. (b) Zoom Map of the study zone, Gray dots are the 1020 seismic stations. The black-dashed line is the railroad (Canadian Pacific Railway). Red and blue crosses are the position

studied. Bottom left inset shows a map of the study area, which is located just north of Marathon, Ontario, Canada. (c) Train seismic record. (d,e) left: stacked section over six trains. (d, e) right: 1 min beamforming panels for six train passages.

of the energy is generated by trains, the quality and spatiotemporal stability of the reconstructed P waves rose. As described in Figure 5, the standard three-step noise-correlation computation

workflow was replaced by a four-step procedure to correlate only the main source of opportune energy, that is, here, trains. Our workflow is as follows:

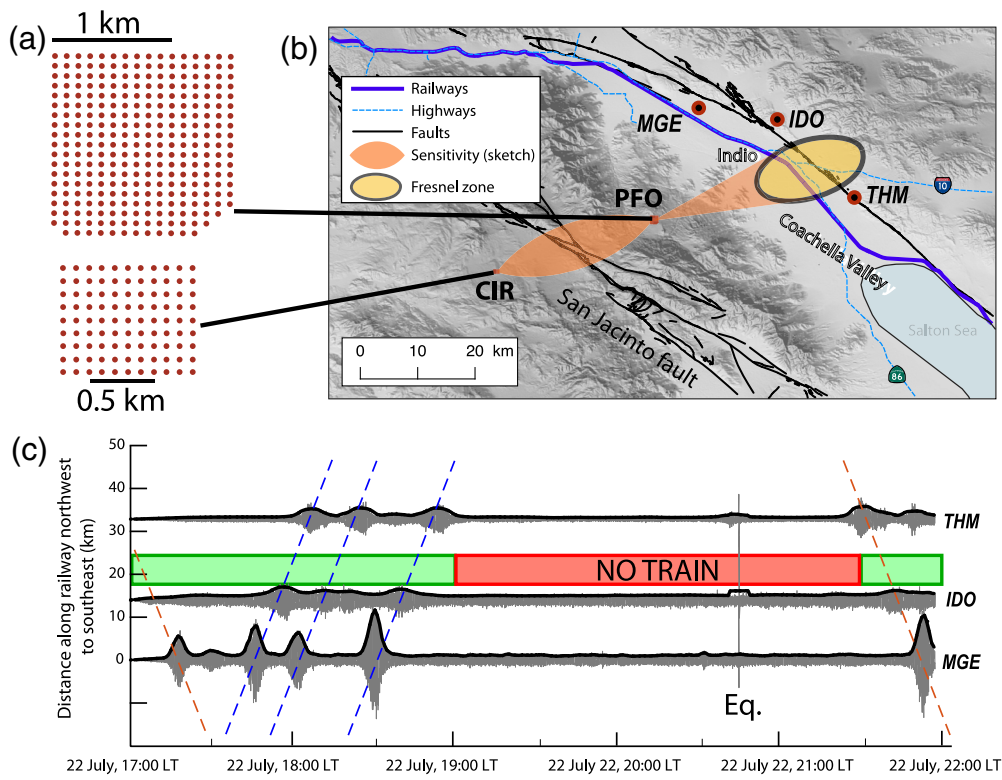


Figure 7. Detection of train passages in the Coachella Valley. (a) Layout of the dense nodal arrays used for the monitoring of the San Jacinto fault. (b) Map of the study area showing the Fresnel zone (yellow ellipse), in which train signals contribute coherently to the P waves in the correlations, traveling between Piñon Flat Observatory (PFO) and Cahuilla Reservation (CIR). Orange areas show the zones of sensitivity to the structure for a wave reconstructed by interferometry between the two arrays. The railway and the main highway are shown in blue. The active tectonic faults are shown in black. The three broadband stations used for building the train catalog are shown with red and black circles. (c) The train catalog is built by slant stacking the envelopes of the train tremors. Colored rectangles show the location of the Fresnel zone along the railway, green for a time window with trains, and red for a time window without a train and rejected from further analysis. The color version of this figure is available only in the electronic edition.

1. First, we built our train catalog for the period of interest (22 July–11 August 2018) using three broadband stations (MGE, IDO, and THM of the CI network, Fig. 7b) near the railway in the Coachella Valley. After band-pass filtering the continuous data between 0.75 and 5 Hz, we slant-stacked the envelopes of the continuous seismograms with apparent velocities of $\pm \sim 95$ km/hr (dashed blue and orange lines in Fig. 7c). This procedure detected trains passing through the stationary phase zone (Fig. 7b) both north-south and south-north.
2. Using the catalog, we sorted broad time windows: those with and without train tremors (large green and red shaded rectangles in Fig. 7c, respectively).
3. In the third step, to analyze the dense nodal array data, we cross correlated the selected time windows (green rectangles in Figs. 7c and 8a), filtered between 3 and 10 Hz and using nonoverlapping data segments of 30 min.

4. We next stacked the cross correlations, according to their interstation separations, into distance-binned correlation gathers. We highlight only correlation gathers for the causal part of the correlations (from PFO to CIR), for a time window centered at the P -wave arrival time. These 30 min correlation gathers were further pruned based on three quality criteria seen in their vespagram, indicators of the different waves' apparent velocities observed in the correlation gathers (Davies *et al.*, 1971). Figure 8b shows the vespagrams associated with the correlation gathers in the upper panels (Fig. 8a). The three quality criteria were (1) SNR1, the ratio between the maximum vespagram amplitude in the (0.13–0.2) s/km slowness (inverse of velocity [5–7.5] km/s velocity) window (dashed black rectangle in the leftmost vespagram panel, Fig. 8b) and the root mean squared (rms) amplitude of the rest of the vespagram. (2) SNR2, the ratio between the maximum vespagram amplitude in the (0.13–0.2) s/km slowness \times (4.5–6) s travel-time window (solid black rectangle in the leftmost vespagram panel, Fig. 8b) and the rms in the rest of the [0.13–0.2] s/km slowness window. (3) Max_{Amp}, the peak vespagram amplitude in the [0.13–0.2] s/km slowness \times (4.5–6) s travel-time window. SNR1 is used to reject gathers exhibiting phases with apparent velocities different from the expected apparent velocity of a direct P wave. SNR2 is used to reject gathers exhibiting energetic spurious phases with arrival times that are either too early or too late, even though their apparent velocity is correct. We used the Max_{Amp} criteria to reject gathers for which the expected P -wave phase is not energetic enough or is too large for a train signal, indicating the detection of an earthquake located in the Fresnel zone (Fig. 8a). For this specific situation, we set thresholds to be sure the conditions $\text{SNR1} \geq 2.5$, $\text{SNR2} \geq 1.5$, and $0.15 \leq \text{Max}_{\text{Amp}} \leq 4.0$ were met for a correlation gather to be selected (green boxes in Fig. 8c). The actual values for

gram amplitude in the (0.13–0.2) s/km slowness \times (4.5–6) s travel-time window (solid black rectangle in the leftmost vespagram panel, Fig. 8b) and the rms in the rest of the [0.13–0.2] s/km slowness window. (3) Max_{Amp}, the peak vespagram amplitude in the [0.13–0.2] s/km slowness \times (4.5–6) s travel-time window. SNR1 is used to reject gathers exhibiting phases with apparent velocities different from the expected apparent velocity of a direct P wave. SNR2 is used to reject gathers exhibiting energetic spurious phases with arrival times that are either too early or too late, even though their apparent velocity is correct. We used the Max_{Amp} criteria to reject gathers for which the expected P -wave phase is not energetic enough or is too large for a train signal, indicating the detection of an earthquake located in the Fresnel zone (Fig. 8a). For this specific situation, we set thresholds to be sure the conditions $\text{SNR1} \geq 2.5$, $\text{SNR2} \geq 1.5$, and $0.15 \leq \text{Max}_{\text{Amp}} \leq 4.0$ were met for a correlation gather to be selected (green boxes in Fig. 8c). The actual values for

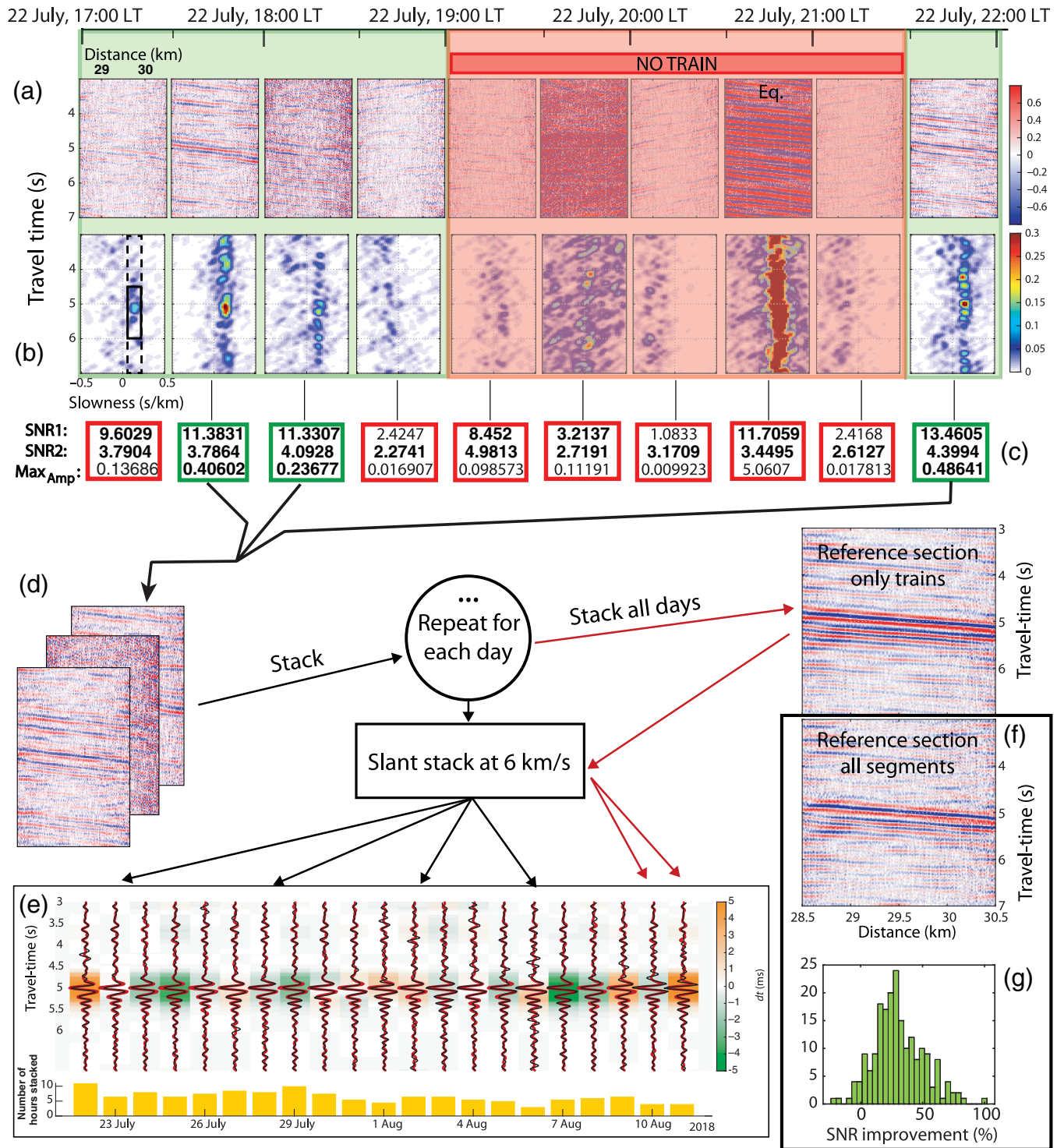


Figure 8. Workflow for monitoring applications. (a) Cross-correlation computation and correlation gathers construction for every 30 min long segments of selected continuous data from the dense arrays. (b) Vespagrams of the correlation gathers used for the 30 min window selection. Black rectangles in the leftmost panel are used to measure the different selection criteria. (c) The three selection criteria associated with each 30 min window. Red boxes are rejected and green boxes are kept for the next step. (d) Stack of the selected 30 min gathers into daily gathers, and

then the daily gathers into the reference gather. (e) Monitoring results. The bottom histogram shows the number of hours of continuous noise records stacked to obtain the daily correlation gathers. (f) Stack of every 30 min windows without train selection, similar to the section shown in Brenguier *et al.* (2019). (g) Histogram of the signal-to-noise ratio (SNR) improvement between the reference correlation gathers without and with train signal selection.

SNR1, SNR2, and Max_{Amp} are shown below each vespagram in Figure 8a.

5. In the last step, we stacked the selected correlation gathers into daily gathers and a reference gather including every selected gather for the whole period of interest (Fig. 8d). Ultimately, we used less than 20% of the full dataset for the monitoring measurements (Fig. 8e). To quantify the improvement of the signals using the opportune sources approach, we measured the ratio of SNRs between a reference gather computed with all of the data (Fig. 8f), similar to Brenguier *et al.* (2019), and the reference gather from selected train windows shown in Figure 8d. We performed this operation for each waveform in the gathers. The results (Fig. 8g) show that the opportune source concentration improves the SNR of the *P*-wave signal by an average of more than 25%. This has important implications for monitoring. As Silver *et al.* (2007) showed, the SNR is the main factor controlling the precision of a time-delay measurement between two similar waveforms; such precision scales linearly with the SNR. Therefore, carefully selecting train signals before correlation allows us to improve the precision of the monitoring measurements. The 30 min long segments of continuous data used here to discretize the study period could be decreased and adapted even more closely to the train signals, which in turn should allow for even larger SNR improvements. This final process is still ahead of us, but the methodology proved effective.
6. The final step of the workflow was to measure seismic velocities. Different approaches were available. We chose to measure relative time shift between the seismograms resulting from the slant stack at 6 km/s of the daily gathers and the reference gather (black and red traces in Fig. 8e, respectively). We measured the instantaneous time delay $\delta t(t)$ between the traces in the 3–10 Hz frequency band using the cross-wavelet transform algorithm of Mao *et al.* (2020). Although a time delay was determined for each sample of the waveform, we only show δt values for the direct *P* wave. Here, the time shifts that we found are shorter than 0.1% of the propagation time, corresponding to time shifts shorter than 5 ms between the daily and reference seismograms. These time shifts can be translated into relative velocity changes with the relation $\delta v/v = -\delta t/t$, using the absolute travel time t of the slant stacked *P* wave. We obtained velocity changes on the order of $\pm 0.1\%$. The meaning of these values is difficult to know because it will take a lot more work to understand the exact sensitivity of the reconstructed *P* wave and the different trade-offs among the source and structure sensitivities (see Fig. 4). We plan to estimate 3D spatial sensitivity kernels for these retrieved travel-time perturbations and correct for shallow, environmental velocity changes. Thus, we shall see whether we will soon be observing and locating any places where changes in seismic velocity at a few kilometers depth occur within the SJFZ.

Discussion and Conclusions

We see great opportunity for exploiting any available massive freight train noise recovery to improve crustal imaging and monitoring dramatically. We describe applications to North America, but our conclusions have global ramifications, especially in such countries and regions as China, Europe, Japan, and India. All have large freight railway systems, often with high-speed passenger lines too. The latter are lighter than freight trains and generate less energetic tremors, but applications might be found in near-surface environmental or engineering studies.

For all of its potential, to put heavy freight train noise to work for seismic imaging and monitoring reasons is of course limited to regions near railways. It also requires trains traveling at rather high speed. However, in general, this article presents a workflow for using other and more local sources of cultural noise, including car and truck traffic, wind farms, and natural sources such as surf break or tectonic, volcanic tremor, as opportune sources of useful seismic noise.

Although promising, this work poses important, practical challenges that the field must confront. Most important is to improve understanding of the retrieved body and surface waves' spatial sensitivity to crustal structures when combining seismic interferometry with opportune sources. In contrast to actively controlled and placed sources, measurements of travel times or temporal travel-time perturbations using more irregular sources not only can improve sensitivity to the structure between the receivers but also can blur the overall picture due to interference between the noise source and the receivers. This latter downside may induce misleading interpretations of velocity or velocity change measurements.

A drawback of examples in this article is that they used so many sensors (hundreds). Train vibrations cost seismologists nothing, but recording them is not yet easy. One solution to overcome these limitations is to find a way to use permanent, single seismic stations instead of costly temporary arrays. One potential initial approach is to deploy dense but temporary seismic arrays around permanent seismic stations. This may help identify useful phases emanating from noise correlations of opportune sources. A hope is that we learn enough to extract the needed information on a long-term basis with permanent stations alone.

One additional major advance would be to couple distributed acoustic sensing data (Zhan, 2020) to seismic interferometry with opportune sources, as described by Dou *et al.* (2017) for car traffic and near-surface applications. This indicates the potential for reconstructing widespread virtual sources along fiber optics from correlations of both short- and long-range opportune sources. Success will open the path to many applications including water-resource management in the near surface and earthquake studies at greater depth.

Data and Resources

The Marathon dataset will be released under DOI: [10.7914/SN/6L_2018](https://doi.org/10.7914/SN/6L_2018). It will either be hosted online or freely sent on external hard

disks upon request via the website for passive seismic techniques for environmentally friendly and cost-efficient mineral exploration (PACIFIC; <https://www.pacific-h2020.eu>). The San Jacinto array data are available on request to F. B. The broadband seismic data used in this study originate from the Southern California Earthquake Center, Caltech. Dataset, DOI: [10.7909/C3WD3xH1](https://doi.org/10.7909/C3WD3xH1). Open-source codes reproducing the results shown in Lavoué *et al.* (2020) are available at https://gricad-gitlab.univ-grenoble-alpes.fr/pacific/publications/2020_Lavoue-et-al_SRL_supplemental-material. Maps are made with Natural Earth. Free vector and raster map data are available at <https://www.naturalearthdata.com>. Figure 3 is based on a map published by the U.S. Department of Transportation (<https://railroads.dot.gov/sites/fra.dot.gov/files/inline-images/0209.png>), built from the (confidential) waybill samples 2010 established by the U.S. Surface Transportation Board, which we could unfortunately not access directly. Coachella Valley train video can be found at https://www.youtube.com/watch?v=pEOLYuf7_F8. Data about public waybill samples are available at <https://prod.stb.gov/wp-content/uploads/PublicUseWaybillSample2018.zip>. Information about University of California Natural Reserve System Boyd Deep Canyon Desert Research Center Reserve is available at DOI: [10.21973/N3V66D](https://doi.org/10.21973/N3V66D). All websites were last accessed in December 2020.

Acknowledgments

The authors acknowledge Nick Arndt, Meysam Rezaeifar, Olivier Coutant, John McBride, Christopher Johnson, Pieter Share, and Florian Fuchs for useful discussions and for supporting data acquisition. This work received funding from the European Union's Horizon 2020 research and innovation program under Grant Agreement Number 776622 (passive seismic techniques for environmentally friendly and cost-efficient mineral exploration [PACIFIC]), from the European Research Council (ERC) under Grant Agreement Number 817803 (FaultScan) and from the Department of Energy (Award DE-SC0016520). The authors are grateful to the reviewers for their useful comments. This work was performed in part at the University of California Natural Reserve System Boyd Deep Canyon Desert Research Center Reserve (see [Data and Resources](#)). The authors gratefully acknowledge the Cahuilla Band of Mission Indians Reservation for graciously allowing us to deploy instruments on tribal land.

References

- Aki, K. (1957). Space and time spectra of stationary stochastic waves, with special reference to microtremors, *Bull. Earthq. Res. Inst., Univ. of Tokyo* **35**, no. 3, 415–456.
- Bakulin, A., and R. Calvert (2006). The virtual source method: Theory and case study, *Geophysics* **71**, no. 4, SI139–SI150.
- Bensen, G., M. Ritzwoller, M. Barmin, A. L. Levshin, F. Lin, M. Moschetti, N. Shapiro, and Y. Yang (2007). Processing seismic ambient noise data to obtain reliable broad-band surface wave dispersion measurements, *Geophys. J. Int.* **169**, no. 3, 1239–1260.
- Boué, P., P. Poli, M. Campillo, H. Pedersen, X. Briand, and P. Roux (2013). Teleseismic correlations of ambient seismic noise for deep global imaging of the Earth, *Geophys. J. Int.* **194**, no. 2, 844–848, doi: [10.1093/gji/ggt160](https://doi.org/10.1093/gji/ggt160).
- Brenguier, F., P. Boué, Y. Ben-Zion, F. Vernon, C. W. Johnson, A. Mordret, O. Coutant, P. E. Share, E. Beaucé, D. Hollis, *et al.* (2019). Train traffic as a powerful noise source for monitoring active faults with seismic interferometry, *Geophys. J. Int.* **46**, no. 16, 9529–9536.
- Brenguier, F., R. Courbis, A. Mordret, X. Campman, P. Boué, M. Chmiel, T. Takano, T. Lecocq, W. Van der Veen, S. Postif, *et al.* (2020). Noise-based ballistic wave passive seismic monitoring. Part 1: Body waves, *Geophys. J. Int.* **221**, no. 1, 683–691.
- Campillo, M., and A. Paul (2003). Long-range correlations in the diffuse seismic coda, *Science* **299**, no. 5606, 547–549, doi: [10.1126/science.1078551](https://doi.org/10.1126/science.1078551).
- Chang, J. P., S. A. L. de Ridder, and B. L. Biondi (2016). High-frequency Rayleigh-wave tomography using traffic noise from Long Beach, California, *Geophysics* **81**, no. 2, B43–B53, doi: [10.1190/geo2015-0415.1](https://doi.org/10.1190/geo2015-0415.1).
- Cheng, Y., Y. Ben-Zion, F. Brenguier, C. W. Johnson, Z. Li, P. E. Share, A. Mordret, P. Boué, and F. Vernon (2020). An automated method for developing a catalog of small earthquakes using data of a dense seismic array and nearby stations, *Seismol. Res. Lett.* **91**, no. 5, 2862–2871.
- Claerbout, J. F. (1968). Synthesis of a layered medium from its acoustic transmission response, *Geophysics* **33**, no. 2, 264–269, doi: [10.1190/1.1439927](https://doi.org/10.1190/1.1439927).
- Connolly, D., G. Kouroussis, O. Lagrouche, C. Ho, and M. Forde (2015). Benchmarking railway vibrations—Track, vehicle, ground and building effects, *Constr. Build. Mater.* **92**, 64–81, doi: [10.1016/j.conbuildmat.2014.07.042](https://doi.org/10.1016/j.conbuildmat.2014.07.042).
- Dales, P., L. Pinzon-Ricon, F. Brenguier, P. Boué, N. Arndt, J. McBride, F. Lavoué, C. J. Bean, S. Beaupretre, R. Fayjaloun, *et al.* (2020). Virtual sources of body waves from noise correlations in a mineral exploration context, *Seismol. Res. Lett.* **91**, no. 4, 2278–2286, doi: [10.1785/0220200023](https://doi.org/10.1785/0220200023).
- Davies, D., E. Kelly, and J. Filson (1971). Vespa process for analysis of seismic signals, *Nat. Phys. Sci.* **232**, no. 27, 8–13.
- Dong, S., J. Sheng, and G. T. Schuster (2006). Theory and practice of refraction interferometry, *SEG Technical Program Expanded Abstracts 2006*, Society of Exploration Geophysicists, 3021–3025.
- Dou, S., N. Lindsey, A. M. Wagner, T. M. Daley, B. Freifeld, M. Robertson, J. Peterson, C. Ulrich, E. R. Martin, and J. B. Ajo-Franklin (2017). Distributed acoustic sensing for seismic monitoring of the near surface: A traffic-noise interferometry case study, *Sci. Rep.* **7**, no. 1, 1–12.
- Douze, E., and S. Laster (1979). Seismic array noise studies at Roosevelt Hot Springs, Utah geothermal area, *Geophysics* **44**, no. 9, 1570–1583.
- Draganov, D., X. Campman, J. Thorbecke, A. Verdel, and K. Wapenaar (2009). Reflection images from ambient seismic noise, *Geophysics* **74**, no. 5, A63–A67.
- Draganov, D., X. Campman, J. Thorbecke, A. Verdel, and K. Wapenaar (2013). Seismic exploration-scale velocities and structure from ambient seismic noise (>1 Hz), *J. Geophys. Res.* **118**, no. 8, 4345–4360.
- Fink, M. (1997). Time reversed acoustics, *Phys. Today* **50**, no. 3, 34–40.
- Fuchs, F., G. Bokelmann, and the AlpArray Working Group (2018). Equidistant spectral lines in train vibrations, *Seismol. Res. Lett.* **89**, no. 1, 56–66, doi: [10.1785/0220170092](https://doi.org/10.1785/0220170092).
- Green, D. N., I. D. Bastow, B. Dashwood, and S. E. Nippes (2017). Characterizing broadband seismic noise in central London, *Seismol. Res. Lett.* **88**, no. 1, 113–124.

- Inbal, A., T. Cristea-Platon, J.-P. Ampuero, G. Hillers, D. Agnew, and S. E. Hough (2018). Sources of long-range anthropogenic noise in southern California and implications for tectonic tremor detection, *Bull. Seismol. Soc. Am.* **108**, no. 6, 3511–3527, doi: [10.1785/0120180130](https://doi.org/10.1785/0120180130).
- King, S., and A. Curtis (2012). Suppressing nonphysical reflections in Green's function estimates using source-receiver interferometry, *Geophysics* **77**, no. 1, Q15–Q25, doi: [10.1190/geo2011-0300.1](https://doi.org/10.1190/geo2011-0300.1).
- Kong, Q., D. T. Trugman, Z. E. Ross, M. J. Bianco, B. J. Meade, and P. Gerstoft (2019). Machine learning in seismology: Turning data into insights, *Seismol. Res. Lett.* **90**, no. 1, 3–14.
- Krylov, V., and C. Ferguson (1994). Calculation of low-frequency ground vibrations from railway trains, *Appl. Acoust.* **42**, no. 3, 199–213, doi: [10.1016/0003-682X\(94\)90109-0](https://doi.org/10.1016/0003-682X(94)90109-0).
- Lavoué, F., O. Coutant, P. Boué, L. Pinzon-Rincon, F. Brenguier, P. Dales, M. Rezaifar, and C. J. Bean (2020). Understanding seismic waves generated by train traffic via modelling: Implications for seismic imaging and monitoring, *Seismol. Res. Lett.* doi: [10.1785/0220200133](https://doi.org/10.1785/0220200133).
- Li, C., Z. Li, Z. Peng, C. Zhang, N. Nakata, and T. Sickbert (2018). Long-period long-duration events detected by the IRIS Community Wavefield Demonstration Experiment in Oklahoma: Tremor or train signals? *Seismol. Res. Lett.* **89**, no. 5, 1652–1659, doi: [10.1785/0220180081](https://doi.org/10.1785/0220180081).
- Mao, S., A. Mordret, M. Campillo, H. Fang, and R. D. van der Hilst (2020). On the measurement of seismic traveltimes changes in the time-frequency domain with wavelet cross-spectrum analysis, *Geophys. J. Int.* **221**, no. 1, 550–568.
- Meng, H., Y. Ben-Zion, and C. W. Johnson (2019). Detection of random noise and anatomy of continuous seismic waveforms in dense array data near Anza California, *Geophys. J. Int.* **219**, no. 3, 1463–1473, doi: [10.1093/gji/ggz349](https://doi.org/10.1093/gji/ggz349).
- Mikesell, D., K. van Wijk, A. Calvert, and M. Haney (2009). The virtual refraction: Useful energy in seismic interferometry, *Geophysics* **74**, no. 3, A13–A17, doi: [10.1190/1.3095659](https://doi.org/10.1190/1.3095659).
- Nakata, N., P. Boué, F. Brenguier, P. Roux, V. Ferrazzini, and M. Campillo (2016). Body and surface wave reconstruction from seismic noise correlations between arrays at Piton de la Fournaise volcano, *Geophys. J. Int.* **43**, no. 3, 1047–1054.
- Nakata, N., J. P. Chang, J. F. Lawrence, and P. Boué (2015). Body wave extraction and tomography at Long Beach, California, with ambient-noise interferometry, *J. Geophys. Res.* **120**, no. 2, 1159–1173, doi: [10.1002/2015JB011870](https://doi.org/10.1002/2015JB011870).
- Nakata, N., R. Snieder, T. Tsuji, K. Larner, and T. Matsuoka (2011). Shear wave imaging from traffic noise using seismic interferometry by cross-coherence, *Geophysics* **76**, no. 6, SA97–SA106, doi: [10.1190/geo2010-0188.1](https://doi.org/10.1190/geo2010-0188.1).
- Olivier, G., F. Brenguier, M. Campillo, R. Lynch, and P. Roux (2015). Body-wave reconstruction from ambient seismic noise correlations in an underground mine, *Geophysics* **80**, no. 3, KS11–KS25, doi: [10.1190/geo2014-0299.1](https://doi.org/10.1190/geo2014-0299.1).
- Poli, P., M. Campillo, H. Pedersen, and LAPNET Working Group (2012). Body-wave imaging of Earth's mantle discontinuities from ambient seismic noise, *Science* **338**, no. 6110, 1063–1065.
- Quiros, D. A., L. D. Brown, and D. Kim (2016). Seismic interferometry of railroad induced ground motions) body and surface wave imaging, *Geophys. J. Int.* **205**, no. 1, 301–313, doi: [10.1093/gji/ggw033](https://doi.org/10.1093/gji/ggw033).
- Riahi, N., and P. Gerstoft (2015). The seismic traffic footprint: Tracking trains, aircraft, and cars seismically, *Geophys. J. Int.* **42**, no. 8, 2674–2681, doi: [10.1002/2015GL063558](https://doi.org/10.1002/2015GL063558).
- Roux, P., K. G. Sabra, W. A. Kuperman, and A. Roux (2005). Ambient noise cross correlation in free space: Theoretical approach, *J. Acoust. Soc. Am.* **117**, no. 1, 79–84.
- Sánchez-Sesma, F. J., and M. Campillo (2006). Retrieval of the Green's function from cross correlation: The canonical elastic problem, *Bull. Seismol. Soc. Am.* **96**, no. 3, 1182–1191.
- Schuster, G., J. Yu, J. Sheng, and J. Rickett (2004). Interferometric/daylight seismic imaging, *Geophys. J. Int.* **157**, no. 2, 838–852.
- Seydoux, L., N. M. Shapiro, J. de Rosny, F. Brenguier, and M. Landès (2016). Detecting seismic activity with a covariance matrix analysis of data recorded on seismic arrays, *Geophys. J. Int.* **204**, no. 3, 1430–1442.
- Shapiro, N. M., M. Campillo, L. Stehly, and M. H. Ritzwoller (2005). High-resolution surface-wave tomography from ambient seismic noise, *Science* **307**, no. 5715, 1615–1618.
- Silver, P. G., T. M. Daley, F. Niu, and E. L. Majer (2007). Active source monitoring of cross-well seismic travel time for stress-induced changes, *Bull. Seismol. Soc. Am.* **97**, no. 1B, 281–293.
- Snieder, R. (2004). Extracting the green's function from the correlation of coda waves: A derivation based on stationary phase, *Phys. Rev. E* **69**, 046610, doi: [10.1103/PhysRevE.69.046610](https://doi.org/10.1103/PhysRevE.69.046610).
- Snieder, R., K. Wapenaar, and K. Larner (2006). Spurious multiples in seismic interferometry primaries, *Geophysics* **71**, no. 4, SI111–SI124, doi: [10.1190/1.2211507](https://doi.org/10.1190/1.2211507).
- Takano, T., F. Brenguier, M. Campillo, A. Peltier, and T. Nishimura (2020). Noise-based passive ballistic wave seismic monitoring on an active volcano, *Geophys. J. Int.* **220**, no. 1, 501–507.
- Tsuji, S., K. Yamaoka, R. Ikuta, T. Kunitomo, T. Watanabe, Y. Yoshida, and A. Katsumata (2018). Secular and coseismic changes in S-wave velocity detected using ACROSS in the Tokai region, *Earth Planets Space* **70**, no. 1, 1–10.
- Wapenaar, K. (2004). Retrieving the elastodynamic Green's function of an arbitrary inhomogeneous medium by cross correlation, *Phys. Rev. Lett.* **93**, no. 25, 254,301.
- Wapenaar, K., and J. Fokkema (2006). Green's function representations for seismic, *Geophysics* **71**, no. 4, SI33–SI46, doi: [10.1190/1.2213955](https://doi.org/10.1190/1.2213955).
- Wapenaar, K., D. Draganov, R. Snieder, X. Campman, and A. Verdel (2010). Tutorial on seismic interferometry: Part 1—Basic principles and applications, *Geophysics* **75**, no. 5, 75A195–75A209.
- Wapenaar, K., E. Slob, R. Snieder, and A. Curtis (2010). Tutorial on seismic interferometry: 2—Underlying theory and new advances, *Geophysics* **75**, no. 5, 75A211–75A227.
- Zhan, Z. (2020). Distributed acoustic sensing turns fiber-optic cables into sensitive seismic, *Seismol. Res. Lett.* **91**, no. 1, 1–15.
- Zhou, W., and H. Paulsen (2020). Compaction of the Groningen gas reservoir investigated with train noise, *Geophys. J. Int.* **223**, doi: [10.1093/gji/ggaa364](https://doi.org/10.1093/gji/ggaa364).

Manuscript received 17 July 2020
Published online 20 January 2021